Draft version April 24, 2018
Preprint typeset using LaTeX style AASTeX6 v. 1.0

DO LYα ABSORBERS CO-ROTATE WITH GALAXY DISKS?

David M. French, Bart P. Wakker
Department of Astronomy, University of Wisconsin, Madison, WI 53706, USA

ABSTRACT

We present results of a study comparing the relative velocity of Lyα absorbers to the rotation direction and velocity of nearby galaxy disks. We find...

Keywords: galaxies:intergalactic medium, galaxies:evolution, galaxies:halos, quasars: absorption lines

1. INTRODUCTION

Our current ΛCDM cosmology picture describes galaxies forming hierarchically out of overdensities in the underlying dark matter distribution. As matter is funneled toward a growing galaxy, conservation of angular momentum redistributes the angular momentum in this gas to match that of the halo and underlying dark matter as the gas is shock-heated and slowly cools. As this infalling gas is responsible for birthing and continuing to feed the galaxies, it is expected that the extended gaseous halos should rotate in the same sense as both the galactic disks and dark matter halos. Galaxy rotation curves have been observed to extend at constant velocity out to... (cite...). It becomes increasingly difficult to measure gas rotation much farther from this however as the density rapidly decreases. Within this region the galaxy disks transition into circumgalactic medium (CGM), and eventually the CGM merges with the intergalactic medium (IGM). At what point, however, does the surrounding medium cease to circulate with the galaxy?

HYDRO? simulations such as those by Stewart et al. (2011, 2013) suggests that the bulk CGM kinematics out to (WHAT DISTANCE) may circulate, and that absorption in intervening QSO sightlines should be able to accurately capture this rotation signature. Observational confirmation, however, has be inconclusive. Côté et al. 2005 probed the halos of nine galaxies using *HST* observed background QSOs, finding large warps would be needed to explain the velocity of H I absorbers by an extended rotating disk. Wakker & Savage (2009) compiled a sample of 4 galaxy-QSO systems from the literature, finding only 1/4 of Lyα absorbers appeared to co-rotate with the associated galaxy disk. Approaching the question from a different angle, Bowen et al. (2016) probed the halo of a single galaxy, NGC1097, with 4 nearby QSO sightlines, and suggests that an extended, slowly rotating disk with additional inflowing IGM material best matches observations.

Numerous studies have shown a correlation between equivalent width and decreasing velocity difference between galaxies and IGM absorbers (e.g., French & Wakker 2017, MORE).

To make progress here, we have obtained rotation curves for 12 nearby spiral galaxies which are located within 500 kpc of a background QSO observed by the Cosmic Origins Spectrograph (COS) on *HST*.

We have augmented this new sample with additional galaxies with known rotation velocity and orientation from the literature. In Section 2 we describe the selection and reduction of both SALT and COS spectra. We then discuss each galaxy-QSO system in detail in Section 3, and introduce our halo-velocity model for interpreting these systems in Section 4. In Section 5 we discuss the overall results of this exercise and present a physically-motivated interpretation of these results. See Section 6 for a summary of our results and conclusions.

2. DATA AND ANALYSIS

2.1. *SALT Data*

Our sample contains 12 galaxies observed with the Southern African Large Telescope (SALT) Robert Stobie Spectrograph (RSS) in longslit mode. These 12 were selected from a larger pool of 48 submitted targets by the SALT observing queue. These 48 possible targets were chosen for their proximity to background QSOs whose spectra contained promising Lyα lines. Finally, we only included galaxies with $z \leq 0.33$ ($cz \leq 10,000$ km s^{-1}), angular sizes less than 6' to enable easy sky subtraction without taking additional exposures, and surface brightnesses sufficient to keep exposure times below $\sim 1300s$. Table 2 summarizes these observations. Data was taken for 2 additional galaxies, NGC3640 and NGC2962, but proved unusable due to issues with spectral identification and low signal-to-noise (respectively).

All SALT galaxy spectra were reduced and extracted using the standard PySALT reduction package (**CITATION**), which includes procedures to prepare the data, correct for gain, cross-talk, bias, and overscan, and finally mosaic the images from the 3 CCDs. Next, we rectify the images with wavelength solutions found via Ne and Ar arc lamp spectra line identification. Finally, we perform a basic sky subtraction using an off-sky portion of the spectrum, and extract 5-10 pixel wide

Target	Galaxy	R.A.	Dec.	z	Program	Cyl. Vel. Range [km s^{-1}]	NFW Vel. Range [km s^{-1}]	T_{exp}* [ks]
(1)	(2)	(3)	(4)	(5)	(6)	(7)	(8)	(9)
1H0419-577	NGC1566	04 26 00.7	-57 12 02.0	0.10400	11686	[49, 77]	[-2, 31]	20429
HE0429-5343	NGC1566	04 30 40.0	-53 36 56.0	0.04001	12275	[-54, -2]	[-22, 17]	2067
HE0435-5304	NGC1566	04 36 50.9	-52 58 47.0	0.42616	11520	[-45, -43]	[-16, -15]	8372
RBS567	NGC1566	04 39 38.7	-53 11 31.0	0.24300	11520	[N/A]	[N/A]	8176
HE0439-5254	NGC1566	04 40 12.0	-52 48 18.0	1.05300	11520	[N/A]	[N/A]	8402
H1101-232	NGC3513	11 03 37.7	-23 29 31.0	0.18600	12025	[-36, 29]	[-35, 33]	13341
SDSSJ112005.00+041323.0	NGC3633	11 20 05.0	+04 13 23.0	0.54689	12603	[-155, -12]	[-77, 13]	4708
RX_J1121.2+0326	CGCG039-137	11 21 14.0	+03 25 47.0	0.15200	12248	[-36, 138]	[-36, 166]	2695
RX_J1121.2+0326	NGC3633	11 21 14.0	+03 25 47.0	0.15200	12248	[-155, -12]	[-77, 13]	2695
SDSSJ112224.10+031802.0	CGCG039-137	11 22 24.1	+03 18 02.0	0.47528	12603	[-130, -114]	[-116, -98]	7588
3C273.0	NGC4536	12 29 06.7	+02 03 09.0	0.15834	12038	[67, 134]	[-6, 43]	4002
HE1228+0131	NGC4536	12 30 50.0	+01 15 23.0	0.11700	11686	[23, 131]	[7, 33]	11036
PG1302-102	NGC4939	13 05 33.0	-10 33 19.0	0.27840	12038	[-219, 14]	[-119, 36]	5979
SDSSJ135726.27+043541.4	NGC5364	13 57 26.3	+04 35 41.0	1.23453	12264	[-38, 123]	[-41, 80]	14148
QSO1500-4140	NGC5786	15 03 34.0	-41 52 23.0	0.33500	11659	[120, 175]	[26, 69]	9258
SDSSJ151237.15+012846.0	UGC09760	15 12 37.2	+01 28 46.0	0.26625	12603	[-30, 30]	[-30,86]	7590
RBS1768	ESO343-G014	21 38 49.9	-38 28 40.0	0.18299	12936	[-203, 10]	[-122, 30]	6962
MRC2251-178	MCG-03-58-009	22 54 05.9	-17 34 55.0	0.06609	12029	[-52, 166]	[-61, 110]	5515
RBS2000	IC5325	23 24 44.7	-40 40 49.0	0.17359	13448	[-46, 5]	[-24, 17]	5046
RX_J1017.5+4702	NGC3198	10 17 31.0	+47 02 25.0	0.33544	13314	[-154, -21]	[-91, 6]	8655
SDSSJ101622.60+470643.0	NGC3198	10 16 22.6	+47 06 43.0	0.82222	11598	[-155, -17]	[-89, 9]	4906
RX_J1236.0+2641	NGC4565	12 36 04.0	+26 41 36.0	0.20920	12248	[-1, 250]	[-29, 146]	4235
PG0804+761	UGC04238	08 10 58.7	+76 02 43.0	0.10200	11686	[-3, 86]	[-6, 94]	5510
SDSSJ104335.90+115129.0	NGC3351	10 43 35.9	+11 05 29.0	0.79400	14071	[-99, 12]	[-68, 20]	4736
MRK771	NGC4529	12 32 03.6	+20 09 30.0	0.06301	12569	[-103, -40]	[-105, -35]	1868
MRK876	NGC6140	16 13 57.2	+65 43 11.0	0.12900	11524	[40, 101]	[35, 102]	12579
SBS1503+570	NGC5907	15 04 55.6	+56 49 20.0	0.35894	12276	[31, 228]	[-24, 101]	5163
SDSSJ152053.59+571122.1	NGC5907	15 20 53.7	+57 11 23.0	0.02952	13654	[-18, 228]	[-42, 114]	3753
RBS1503	NGC5907	15 29 7.5	+56 16 07.0	0.09900	12276	[-228, -9]	[-96, 33]	1964
SDSSJ112448.30+531818.0	UGC06446	11 24 48.3	+53 18 19.0	0.53151	14240	[-9, 65]	[-15, 61]	7920
RX_J1117.6+5301	UGC06446	11 17 40.5	+53 01 51.0	0.15871	14240	[35, 47]	[25, 35]	4943
SBS1116+523	UGC06399	11 19 47.9	+52 05 53.0	0.35568	14240	[-91, -54]†	[-80, -42]†	4949
CSO1208	NGC3726	11 40 47.9	+46 22 05.0	0.11500	14729	[-27, 29]	[-28, 21]	3052
RX_J1142.7+4625	NGC3726	11 42 41.2	+46 24 36.0	0.11500	14772	[-34, -14]	[-30, -7]	2368
3C232	NGC3067	09 58 20.9	+32 24 02.0	0.5306 0	8596	[-121, 25]	[-139, 26]	44662
SDSSJ095914.80+320357.0	NGC3067	09 59 14.8	+32 03 57.0	0.56462	12603	[11, 138]	[-12, 81]	2273
RX_J1002.9+3240	NGC3067	10 02 54.5	+32 40 39.0	0.83000	12603	[115, 147]	[42, 65]	7713
FBQSJ0908+3246	NGC2770	09 08 38.8	+32 46 20.0	0.25989	14240	[-146, -4]	[-132, 6]	7430
SDSSJ091052.80+333008.0	NGC2770	09 10 52.8	+33 30 08.0	0.11631	14240	[6, 145]	[-4, 127]	7442
SDSSJ091127.30+325337.0	NGC2770	09 11 27.3	+32 53 37.0	0.29038	14240	[-150, -43]	[-132, -25]	10028
TON1009	NGC2770	09 09 06.2	+32 36 30.0	0.81028	12603	[-146, -39]	[-125, -20]	4740
TON1015	NGC2770	09 10 37.0	+33 29 24.0	0.35400	14240	[3, 146]	[-7, 130]	4774
CSO295	NGC3432	10 52 05.6	+36 40 40.0	0.60900	14772	[-37, 48]	[-37, 134]	1088
MS1047.3+3518	NGC3432	10 50 10.9	+35 02 02.0	0.04125	8316	[35, 124]	[19, 109]	8301
RX_J1054.2+3511	NGC3432	10 54 16.2	+35 11 24.0	0.20300	14772	[0, 123]	[-9, 111]	533

Table 1. Summary of COS targets in this sample. *Total exposure time and S/N ratio is given for multi-orbit exposures. † Velocity range based on a 2x4 R_{vir} halo.

1-D strips from the reduced 2-D spectrum.

For each 1-D spectrum, we identify the Hα emission lines and perform a non-linear least-squares Voigt profile fit using the Python package LMFIT[1]. The line centroid and 1σ standard errors are returned, and these fits are then shifted to rest-velocity based on the galaxy systemic redshift and heliocentric velocity corrections are calculated with the IRAF rvcorrect procedure. The final rotation velocity is calculated by then applying the inclination correction, $v_{rot} = v/\sin(i)$. Final errors are calculated as a quadrature sum of 1σ fit errors, systemic redshift error, and inclination uncertainty as follows:

$$\sigma^2 = \left(\frac{\partial v_{rot}}{\partial \lambda_{obs}}\right)^2 (\Delta\lambda_{obs})^2 + \left(\frac{\partial v_{rot}}{\partial v_{sys}}\right)^2 (\Delta v_{sys})^2 + \left(\frac{\partial v_{rot}}{\partial i}\right)^2 (\Delta i)^2, \quad (1)$$

where $\Delta\lambda_{obs}$, Δv_{sys}, and Δi are the errors in observed line center, galaxy redshift, and inclination, respectively.

We determine the inclination error by calculating the standard deviation of the set of all axis ratio values available in NED for each galaxy. The final physical scale is calculated using the SALT image scale of 0.1267 arcsec/pixel, multiplied by the 4-pixel spatial binning, and converted to physical units using a redshift-independent distance if available, and a Hubble flow estimate if not. We adopt a Hubble constant of $H_0 = 71$ km s^{-1}Mpc^{-1} throughout.

Finally, we calculate our approaching and receding velocities via a weighted mean of the outer 1/2 of each rotation curve, with errors calculated as weighted standard errors in the mean. Our final redshifts are calculated by forcing symmetric rotation, such that the outer 1/2 average velocity for each side matches in magnitude. See Figure **??** for an example.

2.2. *COS Spectra*

The Barbara A. Mikulski Archive for Space Telescopes (MAST) archives yield 19 QSO targets observed by COS which lie within 500 kpc of our SALT galaxies. These targets vary widely in signal-to-noise from approximately 5 to 100 due to our choosing them based only on their proximity to galaxies with known rotation. The reduction procedure for these spectra follow those described by French & Wakker (2017) and Wakker et al. (2015). In short, spectra are processed with CALCOS vXXXX? and combined via the method of Wakker et al. (2015), which helps corrects the COS wavelength scale misalignments produced by CALCOS. Multiple exposures are combined via alignment with Galactic 21cm absorption spectra and summing total counts per pixel before converting to flux. The COS instrument is described in detail by Green et al. (2012).

[1] http://cars9.uchicago.edu/software/python/lmfit/contents.html

3. HALO ROTATION MODEL

In order to better understand how QSO sightlines probe intervening velocity structure we have developed a simple halo gas rotation model. This model is seeded by an observed rotation curve (or whatever rotation curve-esque data suits ones fancy). This input curve is then interpolated and extended out to $2R_{vir}$ based on the average velocity of the outer 1/2 radius. Next, we project this interpolated rotation curve onto a plane oriented to a faux QSO sightline identically to the input galaxy-QSO pair orientation. By stacking multiple rotation-planes in the galaxy z-axis direction, we then create a simple cylindrical rotating halo model. Finally, each rotation-plane in the stack is projected onto the faux sightline. The result is a function representing the rotation velocity encountered by the sightline as a function of velocity (or distance) along it.

For each galaxy-QSO pair we created 2 rotation models: 1) a purely cylindrical halo extending $2R_{vir}$ in height and $3R_{vir}$ in radius, and 2) a cylindrical model extending $2R_{vir}$ in height and $3R_{vir}$ in radius with rotation velocities which smoothly decline based on a NFW profile fit (Navarro et al. 1996, 1997). Each model produces the velocity a co-rotating absorber would project onto the spectrum as a function of velocity along the sightline. We then collapse this into a simple range of possible observed velocities by summing the x- and y-components along the allowed range.

4. SALT GALAXIES

4.1. *CGCG039-137*

CGCG039-137 is an isolated Scd type galaxy with a measured systemic velocity of 6918 ± 24 km s^{-1} and inclination of 63°. There are two associated sightlines: RX_J1121.2+0326 at an impact parameter of 99 kpc and azimuth angle of 71° on the receding side, and SDSSJ112224.10+031802.0 at 491 kpc and 24° on the approaching side. Lyα absorption is detected in both sightlines within 400km s^{-1} of CGCG039-137.

Towards RX_J1121.2+0326 we detect Lyα at 6975 km s^{-1}, which, at $\Delta v = 57$ km s^{-1}, lies well within the range of projected velocities consistent with co-rotation. The absorber detected toward SDSSJ112224.10+031802.0 occurs at a more distant 6606 km s^{-1}($\Delta v = -312$ km s^{-1}). Although this absorber has the correct sign for co-rotation (blue-ward on the approaching side of the disk), the large velocity difference and impact parameter make it unlikely that this absorption can be linked to coherent halo rotation.

4.2. *ESO343-G014*

ESO343-G014 is an edge on spiral galaxy with a measured systemic velocity of 9138.9 ± 31.7 km s^{-1}. It has a smaller neighboring galaxy, 2MASXJ21372816-3824412,

.

Galaxy	R.A.	Dec.	cz ($\mathrm{km\,s^{-1}}$)	Type	Grating	V_{rot} [$\mathrm{km\,s^{-1}}$]	$V_{rot}/\sin(i)$ [$\mathrm{km\,s^{-1}}$]	Obs Date	T_{exp} [ks]
(1)	(2)	(3)	(4)	(5)	(6)	(7)	(8)	(9)	(10)
CGCG039-137	11 21 26.95	+03 26 41.68	6918 ± 24	Scd	PG2300	132 ± 16	139 ± 26	05 11 2016	700
ESO343-G014	21 37 45.18	−38 29 33.22	9139 ± 32	S	PG2300	203 ± 32	203 ± 32	05 16 2016	1000
IC5325	23 28 43.43	−41 20 0.49	1512 ± 8	SAB(rs)bc	PG2300	53 ± 5	125 ± 39	05 17 2016	600
MCG-03-58-009	22 53 40.85	−17 28 44.00	9015 ± 19	Sc	PG2300	150 ± 12	171 ± 23	05 16 2016	1200
NGC1566	04 20 0.42	−54 56 16.12	1502 ± 15	SAB(rs)bc	PG2300	64 ± 8	195 ± 47	10 18 2016	400
NGC3513	11 03 46.08	−23 14 43.8	1204 ± 12	SB(s)c	PG2300	11 ± 10	22 ± 24	05 26 2016	600
NGC3633	11 20 26.22	+03 35 8.20	2587 ± 7	SAa	PG2300	149 ± 6	157 ± 9	05 11 2016	1200
NGC4536	12 34 27.05	+02 11 17.30	1867 ± 33	SAB(rc)bc	PG2300	129 ± 9	148 ± 41	05 11 2016	1300
NGC4939	13 04 14.39	−10 20 22.60	3093 ± 33	SA(s)bc	PG2300	204 ± 25	275 ± 66	05 14 2016	500
NGC5364	13 56 12.00	+05 00 52.09	1238 ± 17	SA(rs)bc pec	PG2300	130 ± 13	155 ± 22	05 11 2016	700
NGC5786	14 58 56.26	−42 00 48.10	2975 ± 22	SAB(s)bc	PG2300	156 ± 10	172 ± 25	05 11 2016	250
UGC09760	15 12 02.44	+01 41 55.46	2094 ± 16	Sd	PG2300	46 ± 10	46 ± 16	05 11 2016	500

Table 2. SALT targeted galaxies. Columns are as follows: 1) the galaxy name, 2), 3) R.A., Dec. in J2000, 4) galaxy systemic velocity, 5) morphological type (RC3), 6) RSS grating used, 7) approaching side velocity, 8) receding side velocity, 9) observation date, 10) exposure time, and 11) S/N of the Hα or Ca H&K lines.

located north of it's major axis at a projected distance of 216 kpc and velocity of 9129. The nearest sightline is towards RBS1768 at an impact parameter of 466kpc and 74° azimuth angle on the approaching side. We detect 3 Lyα absorption lines within 300 $\mathrm{km\,s^{-1}}$of ESO343-G014 (at 9308, 9360, and 9434 $\mathrm{km\,s^{-1}}$). All of these are anti-aligned with the rotation of ESO343-G014, but unfortunately the presence of 2MASXJ21372816-3824412 makes it difficult to attribute this gas solely to ESO343-G014. Additionally, this gas could be attributed to either the approaching or receding side of the disk due to the large impact parameter and high azimuth angle of the sightline.

4.3. *IC5325*

IC5325 is a face-on SAB(rs)bc type galaxy with a measured velocity of 1511.9 ± 8.4 $\mathrm{km\,s^{-1}}$. It's inclination is just high enough (25°) to obtain a reasonable rotation curve. The closest neighboring galaxy is ESO347-G020 to the Southeast at 306 kpc and a heliocentric velocity of 1745 $\mathrm{km\,s^{-1}}$. Three other much smaller galaxies are also located $\sim$ 450 kpc to the Southwest. We detect Lyα absorption at 1598$\mathrm{km\,s^{-1}}$, $\Delta v = 86\mathrm{km\,s^{-1}}$ in the spectrum towards RBS2000 at an impact parameter of 314 kpc and azimuth angle of 64° on the approaching side. While this velocity is anti-aligned with the rotation the disk gas, the low inclination angle of IC5325 leads to a highly uncertain position angle. Without additional observations, we cannot say for certain if the location of RBS2000 actually lies on the approaching or receding side. This position angle uncertainty also means our SALT rotation curve is a lower limit on the true rotation velocity of IC5325.

4.4. *MCG-03-58-009*

MCG-03-58-009 is a massive and very isolated Sc type galaxy at a measured velocity of 9015 ± 19 $\mathrm{km\,s^{-1}}$ and inclination angle of 49°. A weak Lyα absorber is detected at 9029 $\mathrm{km\,s^{-1}}$ towards MRC2251-178, which lies 355 kpc away at an azimuth angle of 71° on the receding side. Although this absorber matches the velocity direction expected for co-rotation, the velocity difference ($\Delta v = 14$ $\mathrm{km\,s^{-1}}$) is within the systemic velocity uncertainty. The relative weakness of this absorber (EW = 62 ± 4 mÅ) is somewhat surprising given it's proximity (just outside of 1 R_{vir}) to a massive galaxy. If this is representative of an isolated system such as MCG-03-58-009, then we should expect the halo rotational velocity to approach systemic by 1 R_{vir}.

4.5. *NGC1566*

NGC1566 is well sampled (5 nearby QSO sightlines), but unfortunately also part of a complex environment of neighboring galaxies. We detect Lyα in all 5 of these sightlines. The farthest three, HE0439-5254, RBS567, and HE0435-5304, are clustered close together toward the northeast of NGC1566 at 459, 423, and 396 kpc and $\sim$ 60° azimuth angle. HE0439-5254 and RBS567 are both located beyond our 2 x 3 R_{vir} model limits and therefore are only included here for the sake of completeness. The slightly closer HE0435-5304 sneaks under the limit.

HE0429-5343 is in the same direction and azimuth angle but closer at ρ = 256 kpc, and shows Lyα absorption at 1167 and 1358 $\mathrm{km\,s^{-1}}$. These absorbers both have the correct velocity *sign*, but we would expect a smaller velocity for co-rotation (approximately $\Delta v \sim \pm 40$ $\mathrm{km\,s^{-1}}$ projected). This difference could be explained by invoking either a warped extended disk, or perhaps inflowing gas.

1H0419-577 is located to the south at 303 kpc and just east of the receding side of the major axis at an azimuth angle of 10°. We detect Lyα at 1071, 1123, 1188, and 1264 $\mathrm{km\,s^{-1}}$, all of which are the wrong sign for co-rotation or distant in velocity. This sightline is actually

closer to a small group of galaxies including NGC1549, NGC1546 and NGC1536, all with systemic velocities near 1200 km s^{-1}. We expect all of these lines to be associated with this group rather than with NGC1566.

4.6. *NGC3513*

NGC3513 a mostly face-on SB(rs)c galaxy with heliocentric velocity $V_{hel} = 1204 \pm 12$ km s^{-1}. It has a companion galaxy in NGC3511 at an impact parameter of 44 kpc at $v_{hel} = 1109$ km s^{-1}. We detect Lyα at 1182 km s^{-1} toward background QSO H1101-232, which is located directly south at 60 kpc and azimuth angle of 67° on the receding side. NGC3513 appears to be rotating slowly, with a maximal inclination-corrected rotation velocity of 22 ± 24 km s^{-1}. The $\Delta v = -22$ km s^{-1} for this absorber matches well with the magnitude of this rotation, but is opposite in sign for co-rotation. Given that NGC3511 is so close, this absorber's velocity is probably subject to a complex velocity field influenced by both NGC3511 and NGC3513.

4.7. *NGC3633*

NGC3633 is an isolated, edge-on SAa type galaxy at a velocity of 2587 ± 7 km s^{-1}. Several locations along the disk of NGC3633 show two velocities for emission. We have combined these into a single velocity measurement via a weighted average.

There are three nearby sightlines: SDSSJ112005.00+041323.0 is straight north at 468 kpc and 78° azimuth, RX_J1121.2+0326 is to the southeast at 184 kpc and 58° azimuth, and SDSSJ112224.10+031802.0 at 413 kpc and 50° azimuth. Toward RX_J1121.2+0326 we detect a Lyα absorber at 2605 km s^{-1} on the approaching side, which is essentially systemic velocity for NGC3633. The spectrum of SDSSJ112224.10+031802.0 shows absorbers at 2285 and 2578 km s^{-1}, both of which are of the correct sign for co-rotation. We do not detect any Lyα towards the third sightline, SDSSJ112224.10+031802.0.

SDSSJ112005.00+041323.0 and SDSSJ112224.10+031802.0 are both outside of our 2 x 3 R_{vir} model limits.

4.8. *NGC4536*

NGC4536 is a SAB(rs)bc type galaxy located in a complex environment with many other nearby galaxies. The data on the receding side of NGC4536 is quite messy, and may include contamination from background sources. Hence, our measured systemic velocity of 1867±33 km s^{-1}, and thus rotation velocity of 139±37 km s^{-1}, have relatively high uncertainty. Other published redshift values available from NED and rotation velocities from the HyperLEDA database are broadly consistent with our values, albeit biased slightly lower and higher in velocity, respectively.

There are 2 sightlines to the southwest of NGC4536, both on the receding side of the galaxy. HE1228+0131 at 338 kpc and 86° azimuth has 5 Lyα lines: 1495, 1571, 1686, 1721, and 1854 km s^{-1}. None of these are of the correct orientation for co-rotation, and all are more likely to be associated with other nearby galaxies, such as NGC4517A, which is slightly closer to these absorbers in impact parameter and velocity than is NGC4536. The second nearby sightline is toward 3C273 at 344 kpc and 46° azimuth angle, and shows 3 Lyα lines at velocities of 1580, 2156, 2267 km s^{-1}. Two of these are correctly oriented for co-rotation, but are too high in velocity to make this scenario probable. Overall, given the number of nearby galaxies and their locations, we would expect these absorbers to trace the overall velocity field instead of the halo rotation of any particular galaxy.

4.9. *NGC4939*

NGC4939 is a large, fast rotating ($V_{rot} = 275 \pm 49$ km s^{-1}) SA(s)bc type galaxy at systemic velocity $V_{hel} = 3093 \pm 33$ km s^{-1}. We detect a single Lyα absorber at 3448 km s^{-1} towards PG1302-102 at 254 kpc and 61° azimuth angle towards the southeast. This absorber is located on the approaching side of this galaxy, so we can easily rule out co-rotation in this case. NGC4939 does not have any close neighbors, so represents strong case against co-rotation for gas near or past 1 R_{vir}.

4.10. *NGC5364*

NGC5364 is a SA(rs)bc pec type galaxy at a measured systemic velocity of 1238 ± 17 km s^{-1}. It is located in a group environment with 5 other large, nearby galaxies. The sightline toward SDSSJ135726.27+043541.4 at 165 kpc and 84° azimuth angle contains Lyα absorbers at 1124 and 1296 km s^{-1} on the receding side. However, because of the orientation of NGC5364 on the sky with respect to this sightline, these absorbers lie extremely close to the inflection point were projected rotation velocities flip to approaching instead of receding. For example, shifting the location of SDSSJ135726.27+043541.4 east by a tenth of a degree ($\sim$ 20 kpc) is sufficient to put these absorbers on the approaching side of NGC5364. Hence, both of these absorbers could be co-rotating with NGC5364 given very reasonable assumptions on the shape of an extended disk. Nonetheless, the fact that this system lives in galaxy group environment likely dominates the surrounding velocity field.

4.11. *NGC5786*

NGC5786 is a large, strongly-barred spiral galaxy at $V_{sys} = 2975 \pm 22$. The sole nearby sightline lies along the major axis on the receding side of NGC5786 at 453 kpc toward QSO1500-4140. Unfortunately for the purpose of this exercise, there are two neighboring galaxies, both of which are closer than this. ESO327-G038 and ESO327-G039 are both located directly south at 62 kpc and 296 kpc, respectively. Toward QSO1500-4140 we detect Lyα absorption at 3138 km s^{-1} , corresponding to a velocity difference $\Delta v = 163$ km s^{-1}. Although this velocity aligns nicely with expected co-rotation velocities, the nearby neighboring galaxies and large distance

to the absorption ($\sim 2.5R_{vir}$) make it difficult to believe this as evidence of an extended disk.

4.12. *UGC09760*

UGC09760 is an edge-on, slow-rotating Sd galaxy with a single sightline toward SDSSJ151237.15+012846.0 located 123 kpc away along the minor axis. Our measured systemic velocity, $V_{sys} = 2094 \pm 16$, deviates slightly from other published redshifts, such as the The Updated Zwicky Catalog value of $V_{sys} = 2023 \pm 2$ (Falco et al. 1999). This is likely due to our method of imposing rotation symmetry and averaging the approaching and receding velocities to derive V_{sys}. If we do not sample the rotation curve far enough out, a systematic offset is not unreasonable. Indeed, we do not detect the rotation curve turnover or flattening point.

We detect Lyα absorption at 2051 km s^{-1}($\Delta v = -43$ km s^{-1}). This velocity matches well with the rotation velocity of UGC09760 ($V_{rot} = 46 \pm 16$ km s^{-1}), but unfortunately this sightlines lies almost exactly at an azimuth of 90°. Hence, the motion of this gas gas could easily be either co-rotating or counter-rotating depending on a minute change in the position angle assigned to UGC09760. This is especially true if we assume our measured V_{sys} is erroneously high, and indeed closer to the values obtained by other observations.

It is worth noting that there are several small satellite galaxies nearby, including SDSSJ151208.16+013508.5, SDSSJ151121.63+013637.6, SDSSJ151241.38+013723.7 and UGC09746 (impact parameters of 53, 88, 82, 230 kpc respectively). All of these galaxies lie slightly blueward of UGC09760, and thus *farther* away in velocity from the Lyα absorber at 2051 km s^{-1}.

5. ANCILLARY DATA

To increase our sample size we have also searched the literature for galaxies with published rotation curves and orientations. Unfortunately, while the rotation velocity is available for thousands of galaxies, only a handful also include the *orientation* of the rotation on the sky. Of these, we were able to find 18 additional galaxies which have a systemic velocity greater than ~ 500 km s^{-1}, and are near to a COS or STIS sightline with available data.

5.1. *NGC3198*

NGC3198 is a well studied SB(rs)c type galaxy which is included the detailed THINGS rotation curve study of de Blok et al. (2008). We extracted the raw rotation curve derived by de Blok et al. (2008) using the plot digitization software WebPlotDigitizer[2]. NGC3198 has a systemic velocity of 660 km s^{-1}, and is located 370 kpc away from a sightline toward RX_1017.5+4702 at an azimuth angle of 55° on the approaching side of NGC3198 (northeast). NGC3198 has an even and flat rotation curve, with an average velocity of $v_{rot} = 152$ km s^{-1}and an expected velocity range of [-82, -23] based on our projected NFW profile fit. We detect Lyα absorption in the spectrum of RX_1017.5+4702 at 629 km s^{-1}($\Delta v = -31$ km s^{-1}). Hence, the velocity of this absorber can nicely be described by a co-rotating disk.

SDSSJ101622.60+470643.0 is also located in the same direction but at a more distant 401 kpc away (**NOT IDENTIFIED**).

The small dwarf galaxy SDSSJ101848.77+452137.0 is located 65 kpc away toward the southwest.

5.2. *NGC3351*

At $V_{sys} = 778$ km s^{-1}NGC3351 is a mostly face-on ($i = 29°$) SB(r)b type galaxy located $\sim$ 200 kpc southwewst of the core of the Leo I group. We take the rotation curve and orientation produced by Dicaire et al. (2008). While we expect any extended disk rotation to be quickly disrupted due to the complex Leo I environment, this galaxy also has the closest sightline of our sample with SDSSJ104335.90+115129.0 at 31 kpc and 13° azimuth on the northwest, approaching side. We detect Lyα at 717, 882, and 1030 km s^{-1}($\Delta v = -61, 104, 252$ km s^{-1}) toward this sightline. The lowest velocity absorber agrees nicely with both models for co-rotation, while the other two are too high in velocity.

SDSSJ104335.90+115129.0 at 31kpc, 13 az (Lya at 717, 882, 1030)

SDSSJ104816.30+120735.0 at 198kpc, 85 az (G130M but not in reduce)
SDSSJ104709.80+130454.0 at 277kpc, 47 az (G130M but not in reduce)
SDSSJ104843.50+130605.0 at 317kpc, 57 az (G130M but not in reduce)
SDSSJ105220.60+101751.0 at 435kcp, 39 az (not ID'd, possible line)
SDSSJ104341.53+085558.2 at 484kpc, 18 az (G130M but not in reduce)

5.3. *NGC5907*

NGC5907 is a large, edge-on SA(s)c type galaxy at $V_{sys} = 667$ km s^{-1}. We have taken the rotation curve and orientation information from Yim et al. (2014). The closest sightline resides toward SDSSJ152053.59+571122.1 on the northwest (receding) side, at 286 kpc and 63° azimuth.

SDSSJ152053.59+571122.1 at 286 kpc, 63 az (possible line around 880 km s^{-1}, messy spectrum, not ID'd)
SBS1503+570 at 413 kpc, 47 az (Lya at 708kms)
RBS1503 at 478 kpc, 63 az (no lines)

5.4. *NGC4565*

NGC4565 is an edge-on ($i = 75°$ SA(s)b type galaxy at a heliocentric velocity of 1230 km s^{-1}, for which we have taken the rotation curve and orientation from Sofue (1996). The sightline toward RX_J1236.0+2641,

[2] WebPlotDigitizer; http://arohatgi.info/WebPlotDigitizer

at 147 kpc and 41° azimuth angle on receding side, contains Lyα absorbers at velocities of 1009 and 1166 km s^{-1}(Δv = −221, −64 km s^{-1}). Both are consistent with counter-rotating gas, although the line at 1166 km s^{-1}is close to the allowed range of [-29, 146] km s^{-1} for co-rotation. However, the presence of several satellite galaxies surely disrupts any possible extended disk rotation that would otherwise be detectable via sightline absorption.

5.5. *UGC06446*

UGC06446 is an Sd galaxy located at V_{sys} = 645 km s^{-1} on the far northwest edge of the Ursa Major cluster of galaxies. We take the rotation curve and orientation information from (Verheijen & Sancisi 2001; Swaters et al. 2009). We detect Lyα absorption toward two nearby QSO's, SDSSJ112448.30+531818.0 at 143 kpc and 22° azimuth and RX_J1117.6+5301 at 417 kpc and 52° azimuth, are both located toward the southwest, receding side of UGC06446. The absorbers residing at 664 km s^{-1} and 685 km s^{-1}, respectively, both agree well with the expected velocities for co-rotating gas ([-15, 61], [25, 35]). Interestingly, we note that the more distant absorber toward RX_J1117.6+5301 has a larger Δv value (Δv = 40 km s^{-1}compared to 19 km s^{-1}). If both absorbers were strictly following the expected NFW rotation curve, we would expect the opposite, with the more distant absorber velocity approaching V_{sys}.

5.6. *UGC06399*

UGC06399 is an edge-on Sm type galaxy located at V_{sys} = 791 km s^{-1} on the far west edge of the Ursa Major cluster of galaxies. Again, we take the rotation curve and orientation information from (Verheijen & Sancisi 2001; Swaters et al. 2009). As noted by Verheijen & Sancisi (2001), this is the most isolated galaxy in the Ursa Major cluster. Unfortunately, the closest QSO is SBS1116+523, at 471 kpc away on the northwest, approaching side. Although we detect Lyα absorption at 731 km s^{-1}, this impact parameter is beyond our model radius of $3R_{vir}$. Nonetheless, the velocity of this absorber agrees well with the expected velocity range if we extend a static or NFW rotating disk out to $4R_{vir}$.

5.7. *NGC3726*

The third galaxy from the Ursa Major galaxy cluster we're including is NGC3726, a SAB(r)c type galaxy at V_{sys} = 866 km s^{-1}on the southwestern edge of the cluster (Verheijen & Sancisi 2001). Two QSO's, CSO1208 and RX_J1142.7+4625, are located at 369 and 440 kpc, respectively, southeast of NGC3726. They lie very close to and on apposing sides of the minor axis, such that CSO1208 samples the receding side and RX_J1142.7+4625 the approaching. Unfortunately, both are also closer to a small group of dwarf galaxies, including NGC3782 and MCG+08-21-092, ∼ 100 km s^{-1} blueward of NGC3726. We detect Lyα at 731 and 874 km s^{-1} toward CSO1208. The 731 km s^{-1}line is most likely associated with the dwarf group, although the 874 km s^{-1} line falls within the expected range ([-28, 21]) for co-rotating gas.

CSO1208 at 369kpc, 87 az (Lya at 731, 874kms)
RX_J1142.7+4625 (PGC139665) at 440, 86 az (G130M but not in reduce) close to CSO1208

Both sightlines closer to some other little galaxies. NGC3877 nearby, has rot curve

5.8. *NGC3067*

The galaxy-QSO pair NGC3067-3C232 is a particularly well studied system. They are separated by only 11 kpc (74° azimuth angle on NW side) and a LLS of N_{HI} = 110^{20} cm^{-2} is detected toward 3C232 at 1421 km s^{-1}(V_{sys} = 1476 km s^{-1}), which has been postulated as a high velocity cloud (HVC) orbiting NGC3067 (Carilli et al. 1989; Keeney et al. 2005). We obtained the rotation curve for NGC3067 from Rubin et al. (1982) and the orientation from Carilli et al. (1989). While H I measurements of this LLS fit a single component, we have fit 3 separate components at 1408, 1510, and 1641 km s^{-1} to match the associated metal lines (namely, C IV, Si II, Si III, Si IV, Mg II, Fe II, and N I all show at least 2 separate components). This splitting has been analyzed in detail most recently by Keeney et al. (2005) and Stocke et al. (2010), who find similar but slightly lower cz for all three absorbers.

3C232 is located directly north of NGC3067, thus placing it on the receding side. Our NFW model predicts a co-rotating cloud to have a velocity within the range [-139, 26] km s^{-1}. Hence, the 1408 and 1510 km s^{-1}lines can be described as co-rotating (assuming reasonable velocity uncertainties), while the 1641 km s^{-1}line must be either a counter-rotating cloudlet or an outflow directed away from our line of sight.

SDSSJ095914.80+320357.0 at 128 kpc, 43 az (not ID'd, but probable line around 1500kms)
RX_J1002.9+3240 at 359 kpc, 33 az (not in reduce yet)

We have also included the 5 galaxy-QSO systems analyzed by Côté et al. (2005). We briefly summarize each of these systems here, and refer the reader to Côté et al. (2005) for a more complete discussion. **ALL? OF THESE GALAXIES WE PROJECT TO BE AT GREATER IMPACT PARAMETER THAN COTE DID. MOSTLY BASED ON BETTER RID DISTANCES THAN USED BY COTE**

5.9. *NGC6140*

NGC6140 is a small SB(s)cd_pec type galaxy located at V_{sys} = 910 km s^{-1} and 113 kpc from the sightline toward QSO MRK876. The approaching side is oriented toward the east, with MRK876 toward the northwest at an azimuth of 21° (although this is somewhat uncertain; the position angle for NGC6140 could be closer

to 60° than our adopted value of 94° due to it being mostly face on, faint, and strongly barred). We detect Lyα absorption toward MRK876 at 939 km s^{-1}(Δv = 29 km s^{-1}). This value implies co-rotation, but is just below the range predicted by our models (35 - 102 km s^{-1}).

5.10. *NGC4529*

As an inclined, isolated galaxy with a QSO sightline located 159 kpc and only 23° off the major axis, NGC4529 represents an ideal test environment for this study. This sightline towards MRK771 contains a Lyα absorber at 2553 km s^{-1}. With V_{sys} = 2536 km s^{-1} and MRK771 located on the approaching side of NGC4529 (southwest side), this is a clearcut case of counter-rotating H I. As Côté et al. (2005) conclude, "there is simply no physical way to produce such a velocity with an extending co-rotating disk."

5.11. *UGC04238*

UGC04238 is an isolated and edge-on SBd type galaxy at V_{sys} = 1544 km s^{-1}. We take the rotation curve and orientation from Côté et al. (2005). Lyα are detected at 1143, 1526, and 1593 km s^{-1}toward PG0804+761, located directly south at 148 kpc and 59° azimuth on the receding side of UGC04238. Only the absorber at 1593 km s^{-1}, the lowest W of the three, falls within the expected velocity range for co-rotation.

The following are from Rhee & van Albada (1996):

5.12. *NGC2770*

NGC2770 is a large, edge-on Sc type galaxy at V_{sys} = 1947 km s^{-1}. It is mostly isolated except for two nearby small dwarfs MCG+06-20-036NED02 and GALEXASCJ090946.88+330840.4 (both 25 kpc away, on opposite sides of NGC2770). We take the rotation curve and orientation from Rhee & van Albada (1996). There are five nearby QSOs. Toward the south on the approaching side they are the following: FBQSJ0908+3246 at 204 kpc and 59° azimuth (Lyα at 1915, 1982 km s^{-1}), TON1009 at 267 kpc and 41° azimuth (**NEEDS TO BE IDENTIFIED**), and SDSSJ091127.30+325337.0 at 234 kpc and 30° azimuth (Lyα at 2063 km s^{-1}). Only the 1915 km s^{-1} line can reasonably be explained by co-rotation.

Toward the northeast on the receding side they are the following: TON1015 at 218 kpc and 61° azimuth (Lyα at 1833, 1985 km s^{-1}), and SDSSJ091052.80+333008.0 at 239 kpc and 66° azimuth (Lyα at 1824, 1975 km s^{-1}). Two of these lines, at 1985 km s^{-1} and 1975 km s^{-1} are consistent with co-rotation. Interestingly, these two QSO's appear to be sampling the same structures. The absorber pairs at 1833, 1824 km s^{-1} and 1985, 1975 km s^{-1} each have the equivalent EW and $N_{H\,i}$ within errors, and remarkably similar appearing line-structure. Adopting a distance of 28.6 Mpc to this cloud, we calculate a linear separation between TON1015 and SDSSJ091052.80+333008.0 of 28 kpc. Hence, there appears to be two distinct clouds of at least 28 kpc in physical extent sandwiched around the system velocity of NGC2770. **MORE?**

5.13. *NGC3432*

V_{sys} = 616 km s^{-1}. Interacting with the nearby dwarf galaxy UGC05983 located 11 kpc away and at V_{sys} = 765 km s^{-1}. Rhee & van Albada (1996).

Inclination: 78
Adjusted Inc: 90
Morphology: SB(s)m
L_* = 0.42
SW is receding

CSO295 at 20 kpc, 82 az (Lya 600, 662)
RX_J1054.2+3511 at 290 kpc, 57 az (Looks like a feature around 600 km s^{-1} but no ID?)
MS1047.3+3518 at 326 kpc, 26 az (low SN, not ID'd, possible feature?)
SDSSJ110349.70+371527.0 (low res only)

5.14. *NGC3666*

V_{sys} = 1060 km s^{-1}. Mostly isolated, with only a few dwarfs $\sim$ 400 kpc away. Rhee & van Albada (1996)

Inclination: 73
Adjusted Inc: 77
Morphology: SA(rs)c
L_* = 0.61

SDSSJ112439.50+113117.0 at 58 kpc - Borthakur target (Lya at 1047, 1099 km s^{-1})
SDSSJ112632.90+120437.0 at 279 kpc - Borthakur target (not in reduce yet)
SDSSJ112756.70+115427.0 at 320 kpc - (not in reduce yet)
SDSSJ111916.20+110107.0 at 406 kpc - G230L only
4C12.40 at 451 kpc - G190H, G270H, G230L only

5.15. *NGC5951*

V_{sys} = 1780 km s^{-1}. A couple of nearby galaxies (NGC5954, NGC5953), but the sightline is closer and on the opposite side. Rhee & van Albada (1996)

Inclination: 78
Adjusted Inc: 86
Morphology: SBc
L_* = 1.4

2E1530+1511 at 55 kpc, 85 az - (Lya at 1795, 1953)

5.16. *NGC7817*

V_{sys} = 2309 km s^{-1}. Sightline toward MRK335 is equidistant but opposite NGC7798. Rhee & van Albada

(1996)

Inclination: 75
Adjusted Inc: 80
Morphology: SAbc
$L_* = 0.79$

MRK335 at 343 kpc, 90 az (Lya at 1954, 2274)

5.17. *UGC08146*

$V_{sys} = 670$ km s^{-1}. Small but isolated. Rhee & van Albada (1996). This galaxy also is included in the Côté et al. (2005) sample.

Inclination: 78
Adjusted Inc: 90
Morphology: Scd
$L_* = 0.31$

PG1259+593 at 114 kpc, 50 az (Lya at 646, 683)
SBS1304+594 at 235 kpc, 15 az (no lines, low SN)

6. DISCUSSION

7. SUMMARY

8. SIGHTLINES NEEDED

The following targets need to be added:
SBS1304+594
SDSSJ112632.90+120437.0
SDSSJ112756.70+115427.0
RX_J1054.2+3511 - check for feature around 600 km s^{-1}
MS1047.3+3518
TON1009
SDSSJ095914.80+320357.0
RX_J1002.9+3240
RX_J1142.7+4625
SDSSJ152053.59+571122.1
SDSSJ104816.30+120735.0
SDSSJ104709.80+130454.0
SDSSJ104843.50+130605.0
SDSSJ105220.60+101751.0
SDSSJ104341.53+085558.2
SDSSJ101622.60+470643.0

This research has made use of the NASA/IPAC Extragalactic Database (NED) which is operated by the Jet Propulsion Laboratory, California Institute of Technology, under contract with the National Aeronautics and Space Administration. Based on observations with the NASA/ESA *Hubble Space Telescope*, obtained at the Space Telescope Science Institute (STScI), which is operated by the Association of Universities for Research in Astronomy, Inc., under NASA contract NAS 5-26555. **SALT ACKNOWLEDGEMENT**. Spectra were retrieved from the Barbara A. Mikulski Archive for Space Telescopes (MAST) at STScI. Over the course of this study, D.M.F. and B.P.W. were supported by grant AST-1108913, awarded by the US National Science Foundation, and by NASA grants *HST*-AR-12842.01-A, *HST*-AR-13893.01-A, and *HST*-GO-14240 (STScI).

Facility: HST (COS)

APPENDIX

A. ROTATION CURVES

Here we present rotation curves with finder charts indicating the slit position for each galaxy observed with SALT.

REFERENCES

Bowen, D. V., Chelouche, D., Jenkins, E. B., et al. 2016, ApJ, 826, 50
Carilli, C. L., van Gorkom, J. H., & Stocke, J. T. 1989, Nature, 338, 134
Côté, S., Wyse, R. F. G., Carignan, C., Freeman, K. C., & Broadhurst, T. 2005, ApJ, 618, 178
de Blok, W. J. G., Walter, F., Brinks, E., et al. 2008, AJ, 136, 2648
Dicaire, I., Carignan, C., Amram, P., et al. 2008, MNRAS, 385, 553
Falco, E. E., Kurtz, M. J., Geller, M. J., et al. 1999, PASP, 111, 438
French, D. M., & Wakker, B. P. 2017, ApJ, 837, 138
Green, J. C., Froning, C. S., Osterman, S., et al. 2012, ApJ, 744, 60
Keeney, B. A., Momjian, E., Stocke, J. T., Carilli, C. L., & Tumlinson, J. 2005, ApJ, 622, 267
Navarro, J. F., Frenk, C. S., & White, S. D. M. 1996, ApJ, 462, 563
—. 1997, ApJ, 490, 493
Rhee, M.-H., & van Albada, T. S. 1996, A&AS, 115, 407
Rubin, V. C., Thonnard, N. T., & Ford, Jr., W. K. 1982, AJ, 87, 477
Sofue, Y. 1996, ApJ, 458, 120
Stewart, K. R., Brooks, A. M., Bullock, J. S., et al. 2013, ApJ, 769, 74
Stewart, K. R., Kaufmann, T., Bullock, J. S., et al. 2011, ApJ, 738, 39
Stocke, J. T., Keeney, B. A., & Danforth, C. W. 2010, PASA, 27, 256
Swaters, R. A., Sancisi, R., van Albada, T. S., & van der Hulst, J. M. 2009, A&A, 493, 871
Verheijen, M. A. W., & Sancisi, R. 2001, A&A, 370, 765
Wakker, B. P., Hernandez, A. K., French, D. M., et al. 2015, ApJ, 814, 40
Wakker, B. P., & Savage, B. D. 2009, ApJS, 182, 378
Yim, K., Wong, T., Xue, R., et al. 2014, AJ, 148, 127

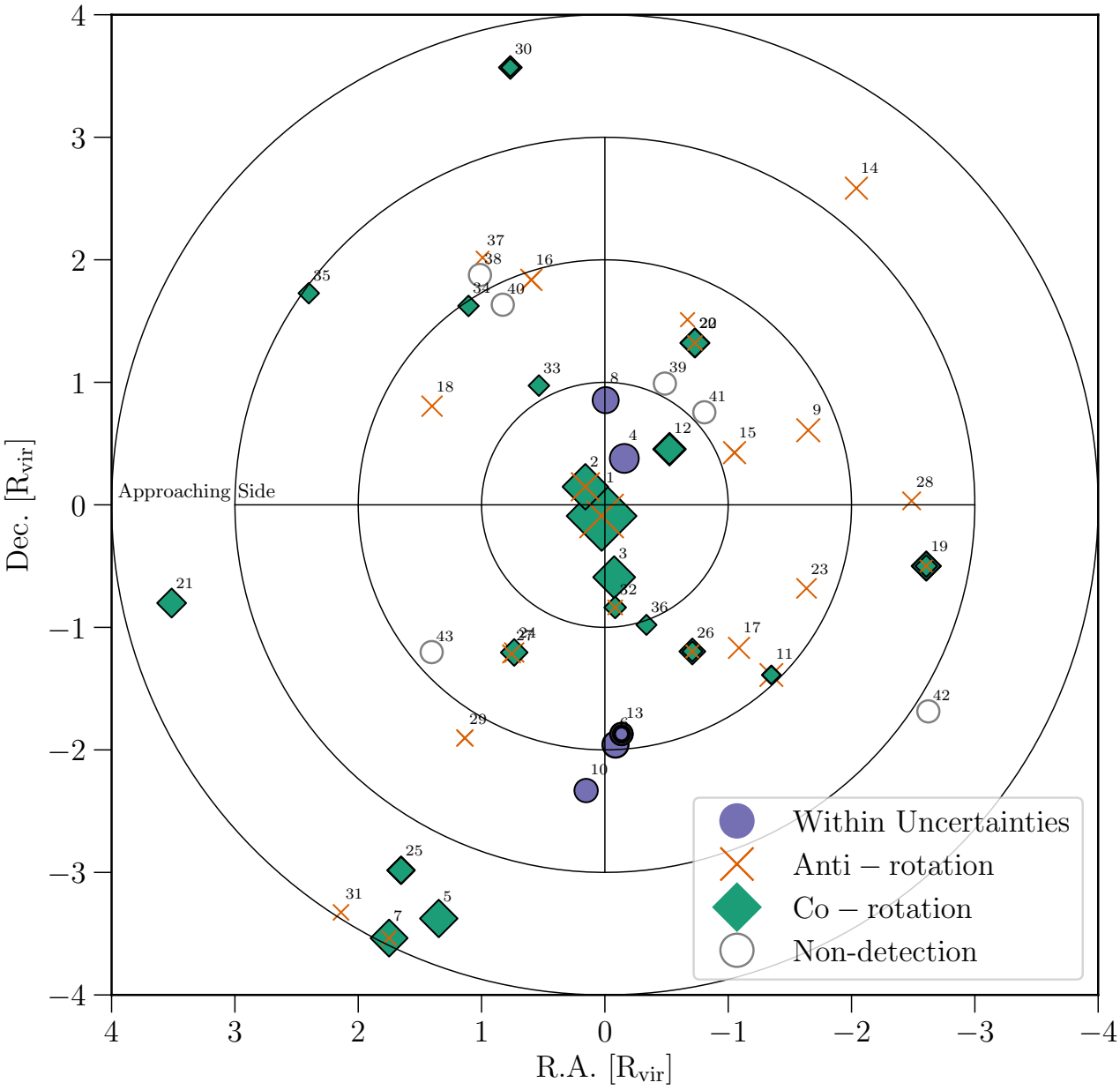

Figure 1. A map of the locations of each absorber normalized with respect to the galaxy virial radius. Concentric rings indicate distances of 1, 2, 3 and 4 R_{vir}. All galaxies are rotated to PA = 90 or 270, such that their major axis' are horizontal and their approaching side is on the left as indicated. The color and style of each point indicates the line-of-sight velocity compared to that of the rotation of the nearby galaxy. Green diamonds indicate co-rotation, red X's indicate anti-rotation, and purple circles indicate cases where either is possible due to a combination of orientation and velocity uncertainties. The size of each point is scaled to reflect the EW of the absorber. The labeled galaxy-QSO pairs are as follows: 1. NGC3067 : 3C232, 2. NGC3351 : SDSSJ104335.90 + 115129.0, 3. CGCG039 − 137 : RX$_J$1121.2 + 0326, 4. NGC3513 : H1101 − 232, 5. NGC1566 : RBS567, 6. NGC3726 : CSO1208, 7. NGC1566 : HE0439 − 5254, 8. UGC09760 : SDSSJ151237.15 + 012846.0, 9. NGC6140 : MRK876, 10. NGC3726 : RX$_J$1142.7 + 4625, 11. NGC4536 : 3C273.0, 12. NGC4565 : RX$_J$1236.0 + 2641, 13. NGC4536 : HE1228 + 0131, 14. UGC06446 : RX$_J$1117.6 + 5301, 15. UGC06446 : SDSSJ112448.30 + 531818.0, 16. ESO343 − G014 : RBS1768, 17. NGC5907 : SBS1503 + 570, 18. NGC2770 : SDSSJ091127.30 + 325337.0, 19. NGC1566 : 1H0419 − 577, 20. NGC2770 : SDSSJ091052.80 + 333008.0, 21. UGC06399 : SBS1116 + 523, 22. NGC2770 : TON1015, 23. NGC4529 : MRK771, 24. NGC2770 : FBQSJ0908+3246, 25. NGC1566 : HE0435−5304, 26. UGC04238 : PG0804+761, 27. NGC3633 : RX$_J$1121.2+0326, 28. NGC5786 : QSO1500 − 4140, 29. NGC1566 : HE0429 − 5343, 30. NGC3633 : SDSSJ112005.00 + 041323.0, 31. NGC4536 : LBQS1230−0015, 32. NGC5364 : SDSSJ135726.27+043541.4, 33. NGC4939 : PG1302−102, 34. NGC3198 : RX$_J$1017.5+4702, 35. CGCG039 − 137 : SDSSJ112224.10 + 031802.0, 36. MCG − 03 − 58 − 009 : MRC2251 − 178, 37. IC5325 : RBS2000, 38. NGC3198 : SDSSJ101622.60 + 470643.0, 39. NGC5907 : SDSSJ152053.59 + 571122.1, 40. NGC5907 : RBS1503, 41. NGC3067 : SDSSJ095914.80 + 320357.0, 42. NGC3067 : RX$_J$1002.9 + 3240, 43. NGC2770 : TON1009

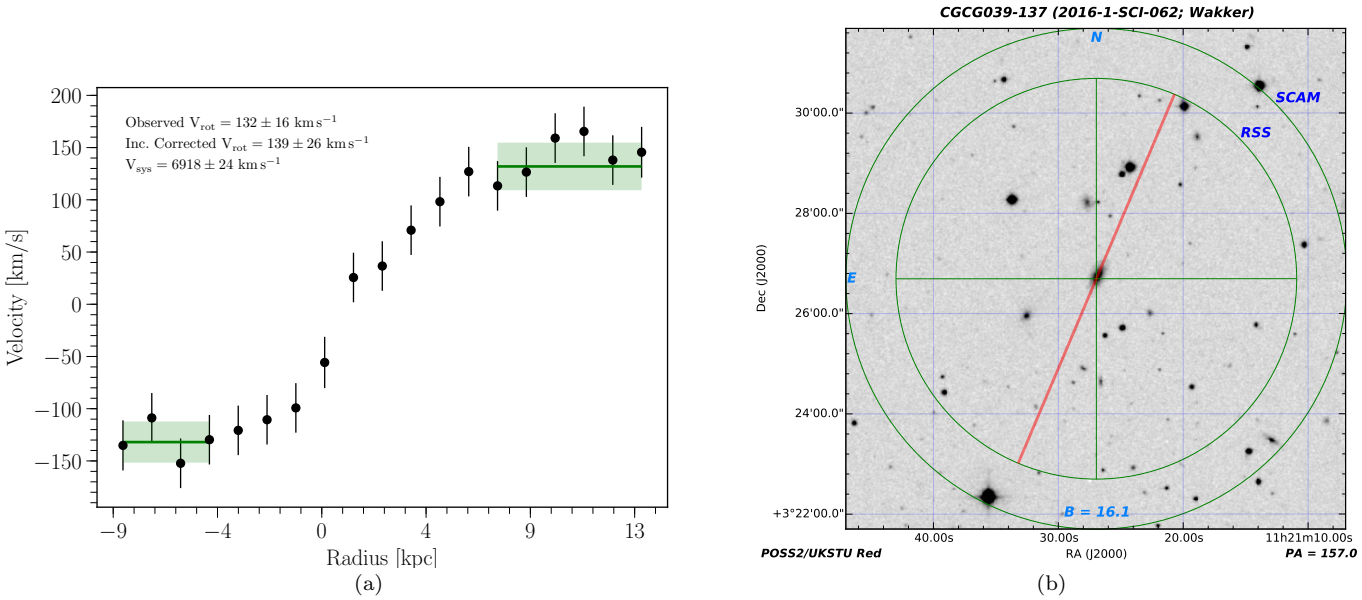

(a) (b)

Figure A1. a) Rotation curve of CGCG039-137. The solid green line indicates the weighted mean velocity over the corresponding x-axis region, and the shaded green indicates the 1σ error in the mean. b) SALT finder chart for CGCG039-137 showing the position of the slit in red.

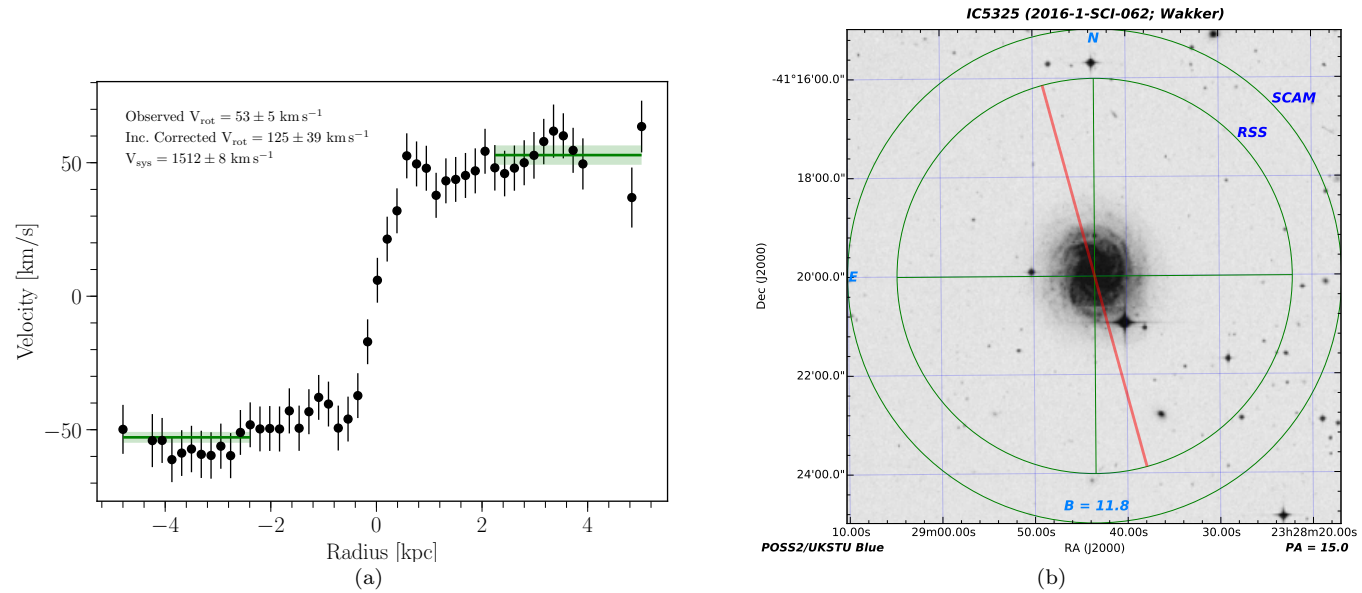

(a) (b)

Figure A2. a) Rotation curve of IC5325. The solid green line indicates the weighted mean velocity over the corresponding x-axis region, and the shaded green indicates the 1σ error in the mean. b) SALT finder chart for IC5325 showing the position of the slit in red.

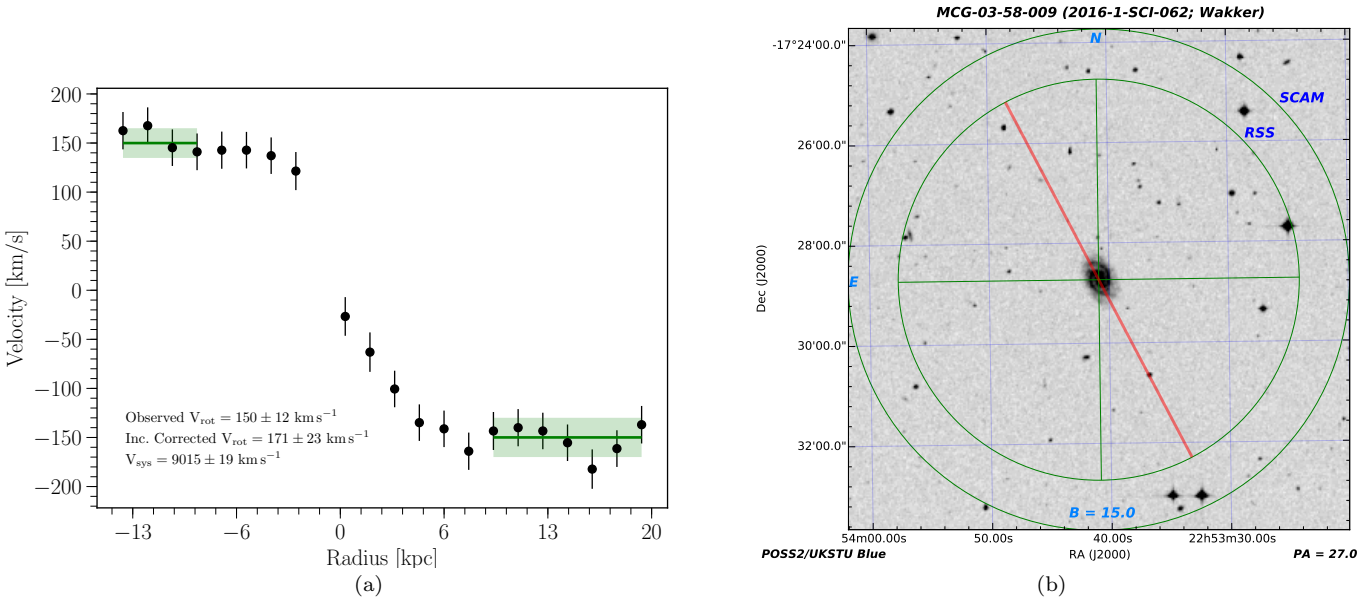

(a) (b)

Figure A3. a) Rotation curve of MCG-03-58-009. The solid green line indicates the weighted mean velocity over the corresponding x-axis region, and the shaded green indicates the 1σ error in the mean. b) SALT finder chart for MCG-03-58-009 showing the position of the slit in red.

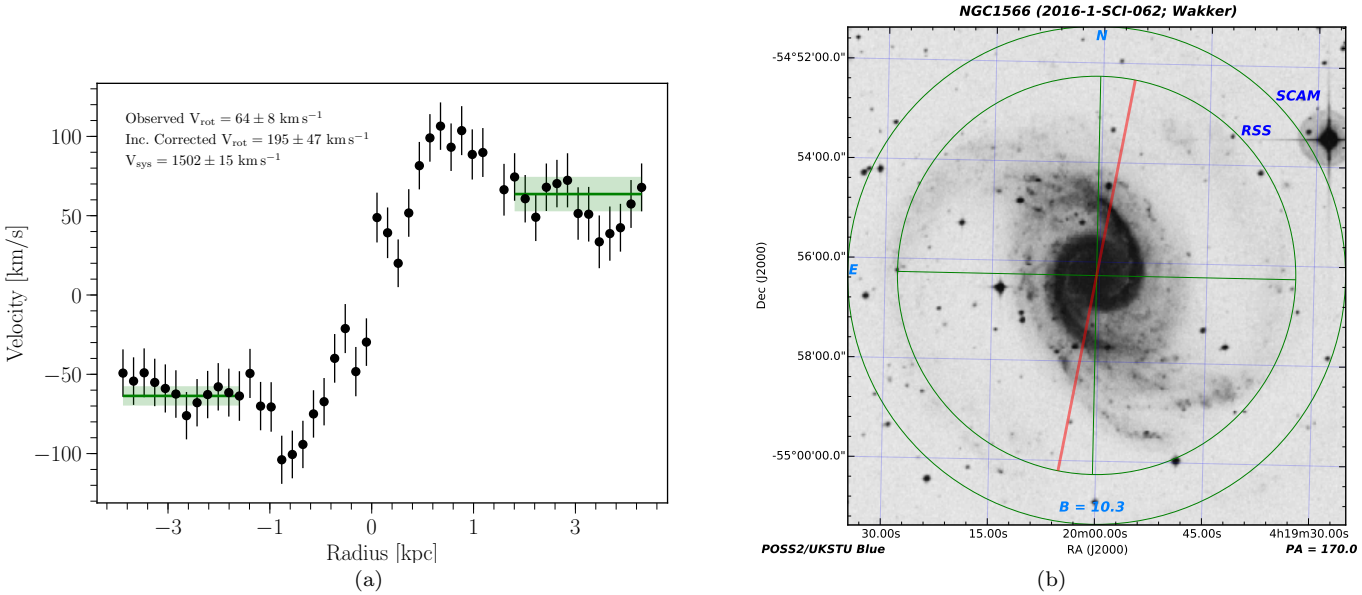

(a) (b)

Figure A4. a) Rotation curve of NGC1566. The solid green line indicates the weighted mean velocity over the corresponding x-axis region, and the shaded green indicates the 1σ error in the mean. b) SALT finder chart for NGC1566 showing the position of the slit in red.

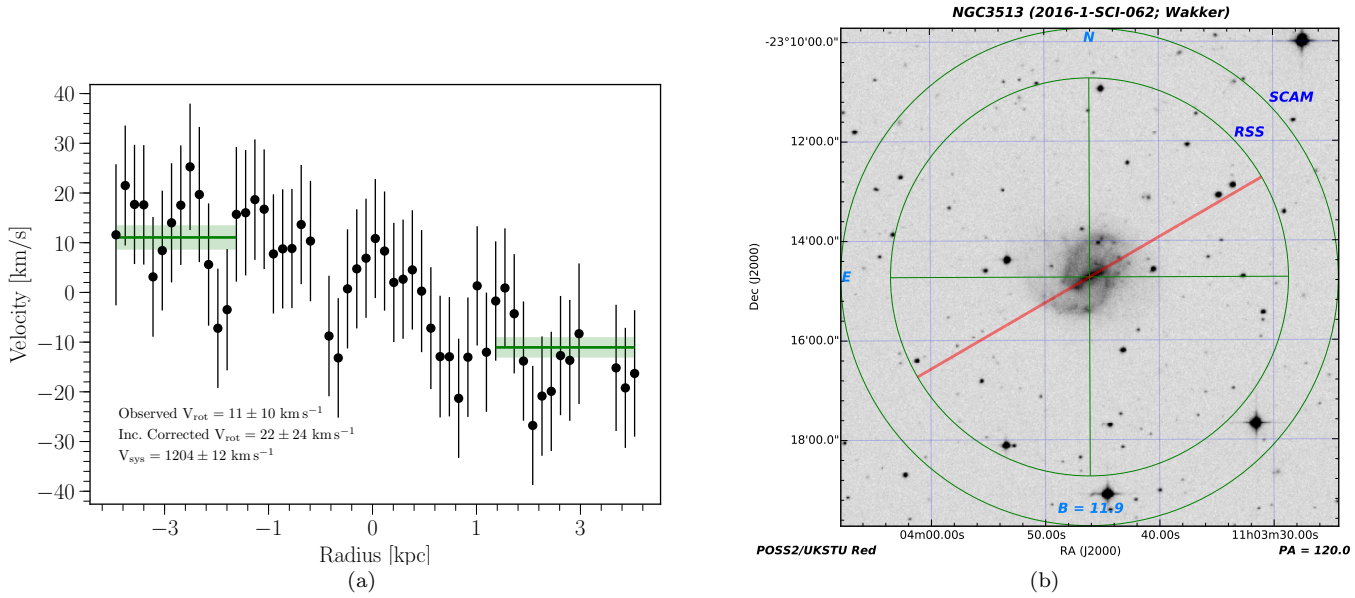

(a) (b)

Figure A5. a) Rotation curve of NGC3513. The solid green line indicates the weighted mean velocity over the corresponding x-axis region, and the shaded green indicates the 1σ error in the mean. b) SALT finder chart for NGC3513 showing the position of the slit in red.

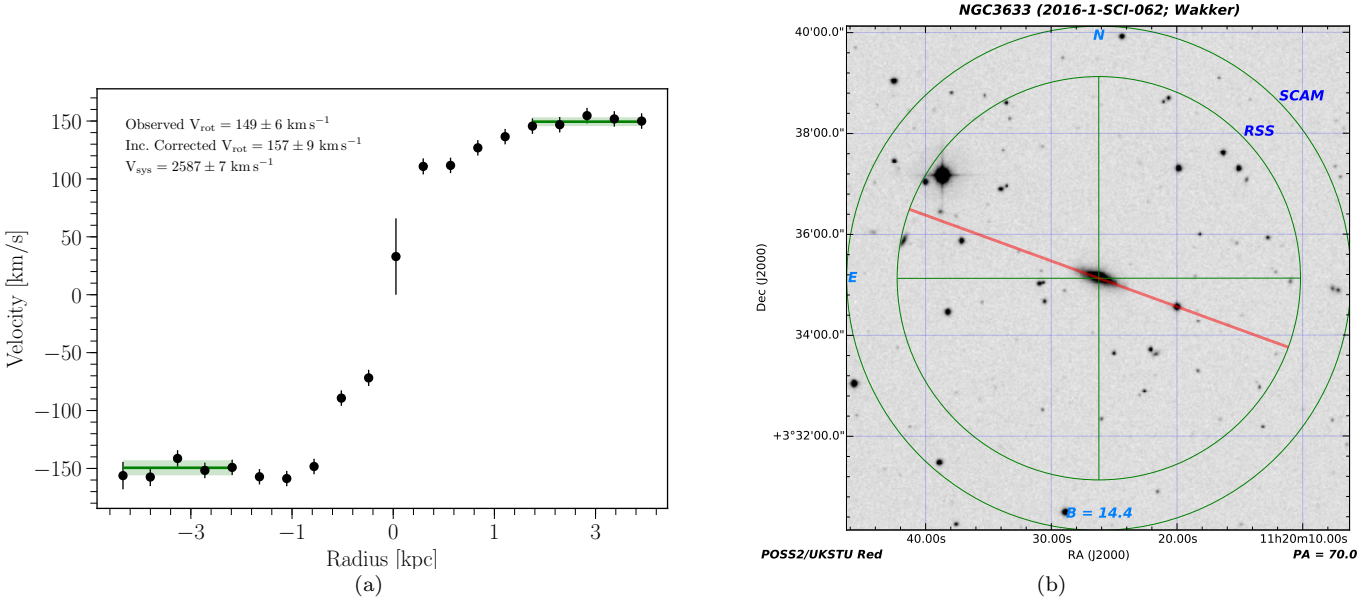

(a) (b)

Figure A6. a) Rotation curve of NGC4536. The solid green line indicates the weighted mean velocity over the corresponding x-axis region, and the shaded green indicates the 1σ error in the mean. b) SALT finder chart for NGC3633 showing the position of the slit in red.

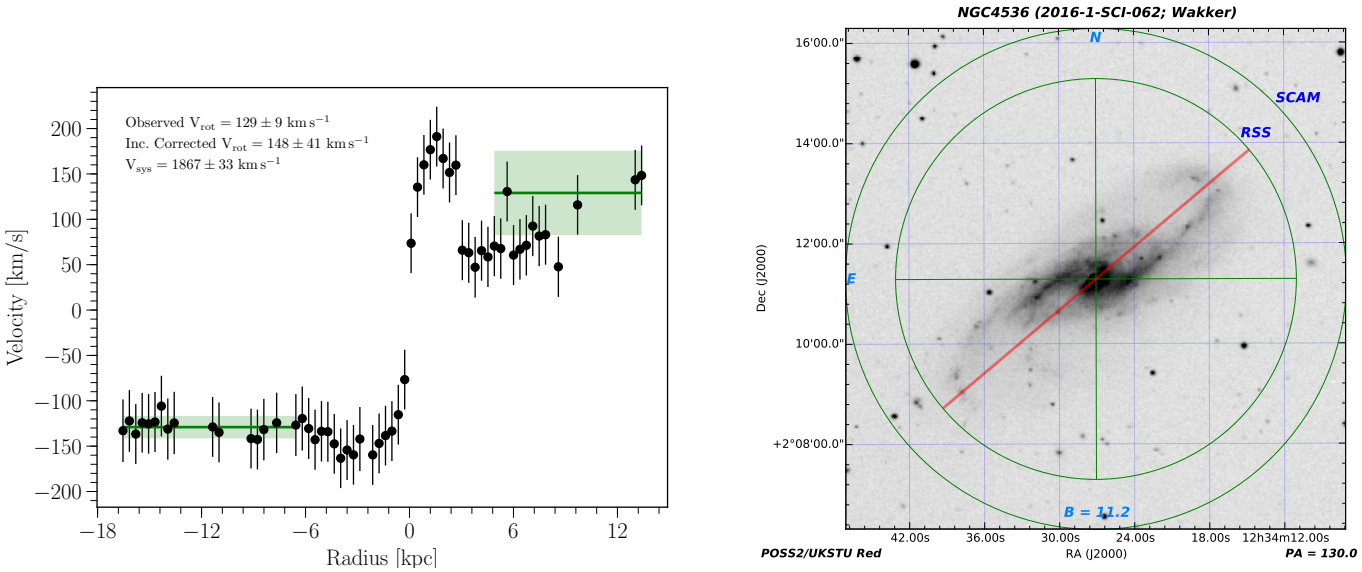

(a) (b)

Figure A7. a) Rotation curve of NGC4536. The solid green line indicates the weighted mean velocity over the corresponding x-axis region, and the shaded green indicates the 1σ error in the mean. b) SALT finder chart for NGC4536 showing the position of the slit in red.

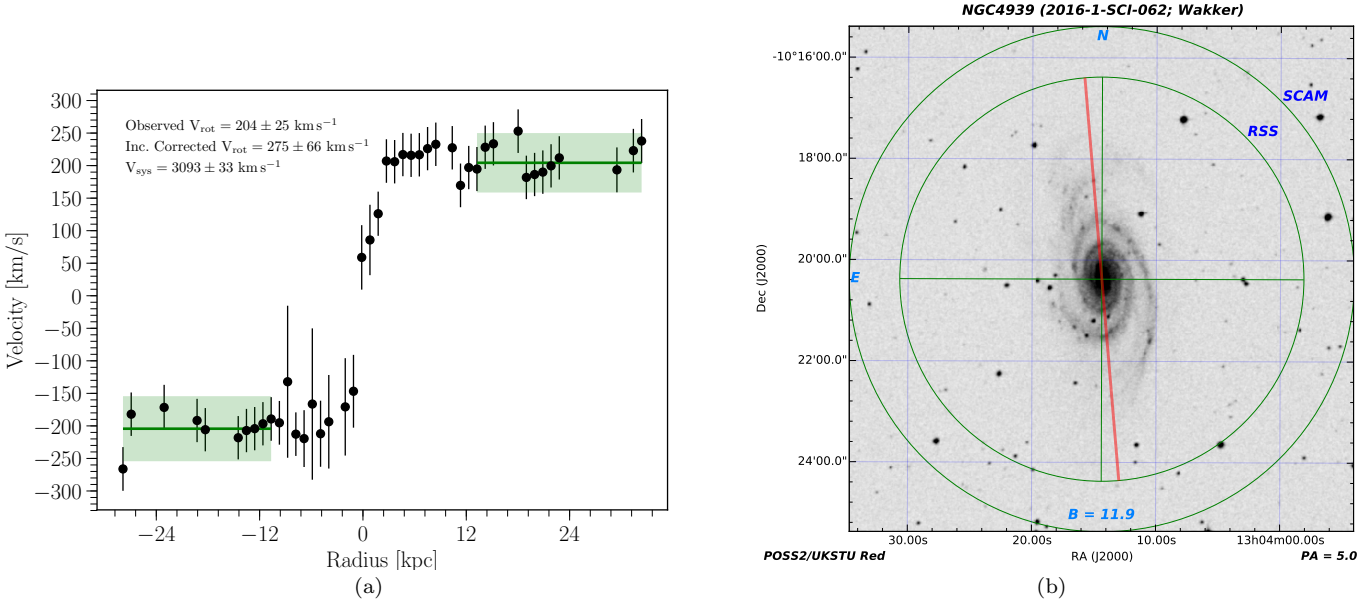

(a) (b)

Figure A8. a) Rotation curve of NGC4939. The solid green line indicates the weighted mean velocity over the corresponding x-axis region, and the shaded green indicates the 1σ error in the mean. b) SALT finder chart for NGC4939 showing the position of the slit in red.

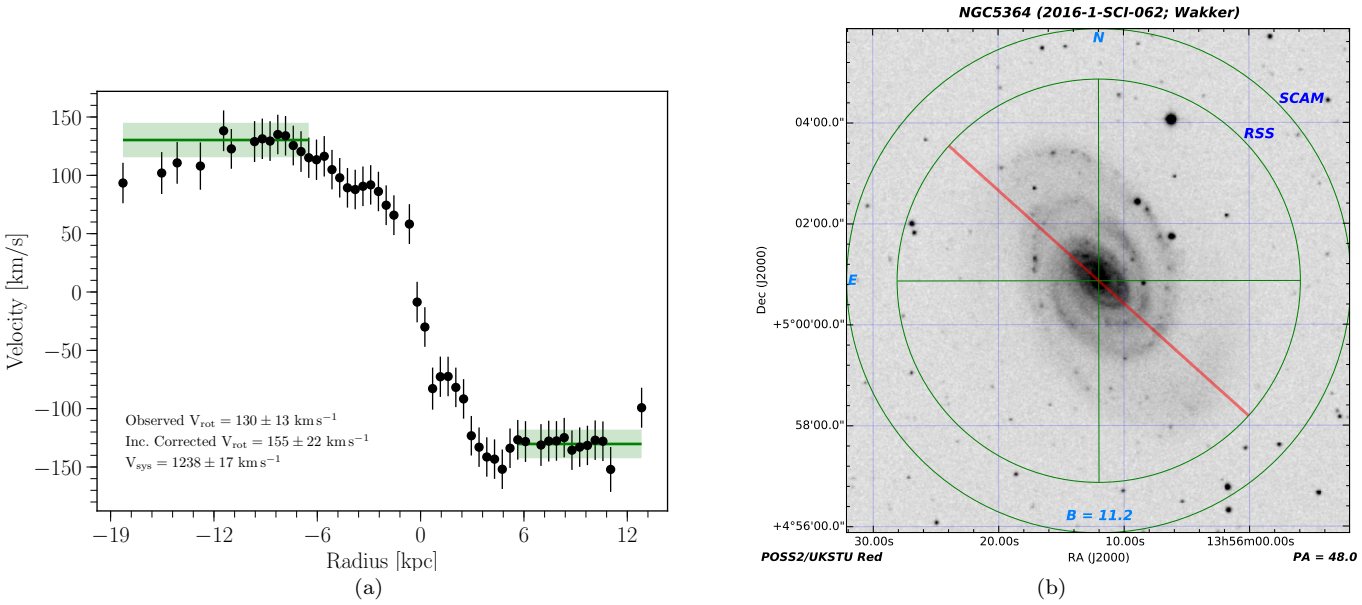

(a) (b)

Figure A9. a) Rotation curve of NGC5364. The solid green line indicates the weighted mean velocity over the corresponding x-axis region, and the shaded green indicates the 1σ error in the mean. b) SALT finder chart for NGC5364 showing the position of the slit in red.

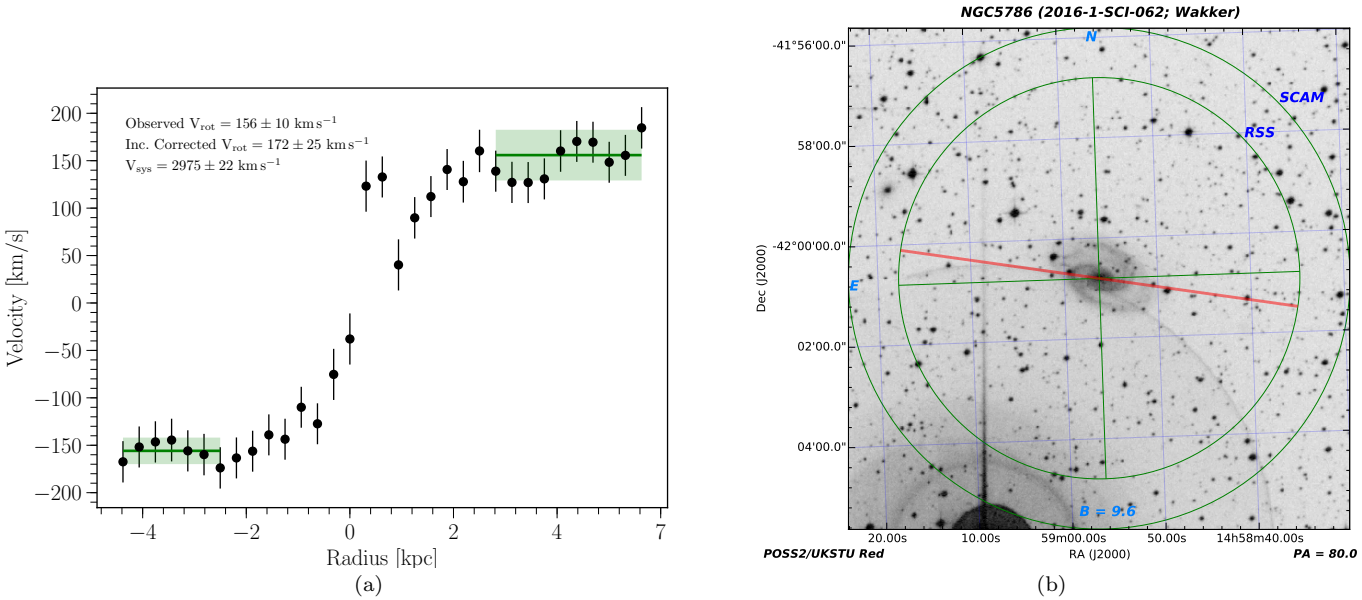

(a) (b)

Figure A10. a) Rotation curve of NGC5786. The solid green line indicates the weighted mean velocity over the corresponding x-axis region, and the shaded green indicates the 1σ error in the mean. b) SALT finder chart for NGC5786 showing the position of the slit in red.

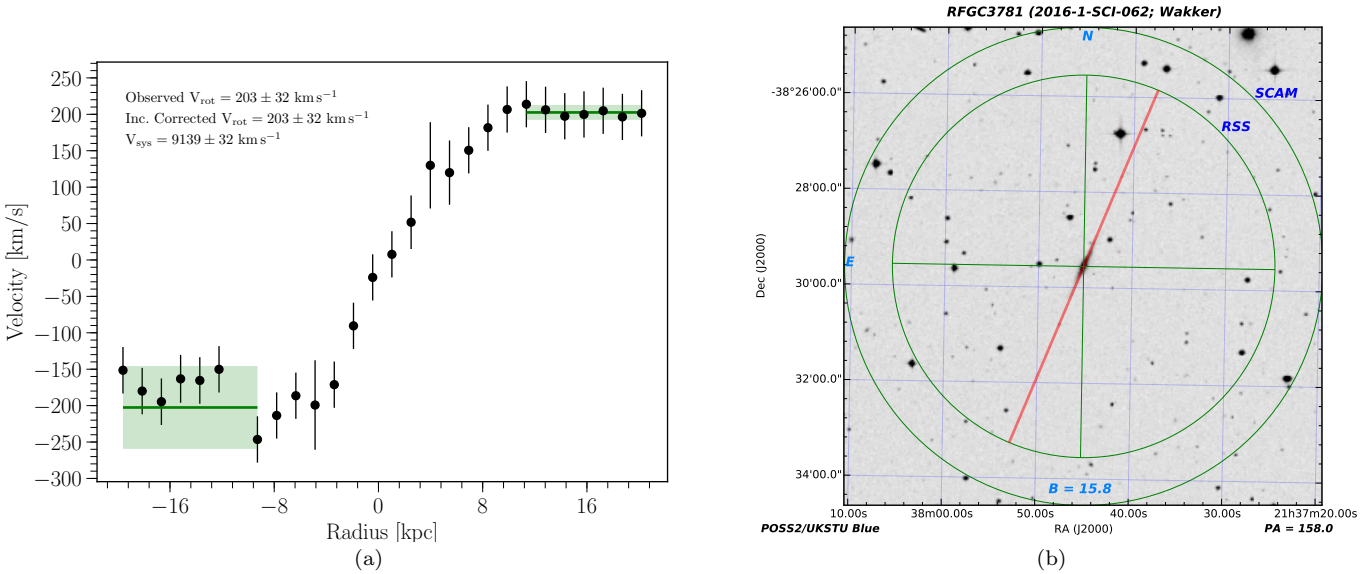

(a) (b)

Figure A11. a) Rotation curve of NGC5364. The solid green line indicates the weighted mean velocity over the corresponding x-axis region, and the shaded green indicates the 1σ error in the mean. b) SALT finder chart for NGC5364 showing the position of the slit in red.